Algal Dual-Specificity Tyrosine Phosphorylation-Regulated Kinase, Triacylglycerol Accumulation Regulator1, Regulates Accumulation of Triacylglycerol in Nitrogen or Sulfur Deficiency[1][OPEN]

Masataka Kajikawa, Yuri Sawaragi, Haruka Shinkawa, Takashi Yamano, Akira Ando, Misako Kato, Masafumi Hirono[2], Naoki Sato, and Hideya Fukuzawa*

Graduate School of Biostudies, Kyoto University, Kyoto 606–8502, Japan (Ma.K., Y.S., H.S., T.Y., H.F.); Graduate School of Humanities and Sciences, Ochanomizu University, Tokyo 112–8610, Japan (A.A., Mi.K.); Graduate School of Science, University of Tokyo, Tokyo 113–0033, Japan (M.H.); and Graduate School of Arts and Sciences, University of Tokyo, Tokyo 153–8902, Japan (N.S.)

ORCID ID: 0000-0003-0963-5662 (H.F.).

Although microalgae accumulate triacylglycerol (TAG) and starch in response to nutrient-deficient conditions, the regulatory mechanisms are poorly understood. We report here the identification and characterization of a kinase, triacylglycerol accumulation regulator1 (TAR1), that is a member of the yeast (*Saccharomyces cerevisiae*) Yet another kinase1 (Yak1) subfamily in the dual-specificity tyrosine phosphorylation-regulated kinase family in a green alga (*Chlamydomonas reinhardtii*). The kinase domain of TAR1 showed auto- and transphosphorylation activities. A TAR1-defective mutant, *tar1-1*, accumulated TAG to levels 0.5- and 0.1-fold of those of a wild-type strain in sulfur (S)- and nitrogen (N)-deficient conditions, respectively. In N-deficient conditions, *tar1-1* showed more pronounced arrest of cell division than the wild type, had increased cell size and cell dry weight, and maintained chlorophyll and photosynthetic activity, which were not observed in S-deficient conditions. In N-deficient conditions, global changes in expression levels of N deficiency-responsive genes in N assimilation and tetrapyrrole metabolism were noted between *tar1-1* and wild-type cells. These results indicated that TAR1 is a regulator of TAG accumulation in S- and N-deficient conditions, and it functions in cell growth and repression of photosynthesis in conditions of N deficiency.

Triacylglycerol (TAG) is a representative neutral lipid that is accumulated as a carbon store in animals, plants, and fungi. Microalgae accumulate TAG as a storage lipid in response to a variety of environmental stress conditions, and such a lipid pool could form the basis of a biofuel resource. The model green alga (*Chlamydomonas reinhardtii*) accumulates significant levels of TAG in nitrogen (N)-deficient (Siaut et al., 2011; Merchant et al., 2012), sulfur (S)-deficient (Boyle et al., 2012; Sato et al., 2014), and phosphate-deficient (Iwai et al., 2014) conditions. Among these conditions, N deficiency is considered as the best trigger of effective TAG accumulation (Boyle et al., 2012; Fan et al., 2012).

Furthermore, exogenously supplied acetate can boost TAG accumulation in N-deficient conditions (Goodson et al., 2011; Fan et al., 2012). Although comprehensive gene and protein expression profiles during responses to N deficiency have been reported in *C. reinhardtii* (Miller et al., 2010; Boyle et al., 2012; Longworth et al., 2012; Blaby et al., 2013; Schmollinger et al., 2014), the regulatory mechanisms involved in TAG accumulation are still largely unclear. So far, the genes *plastid galactoglycerolipid degradation1* (*PGD1*; Li et al., 2012), *nitrogen-responsive regulator1* (*NRR1*; Boyle et al., 2012), and *phospholipid:diacylglycerol acyltransferase1* (*PDAT1*; Boyle et al., 2012; Yoon et al., 2012) have been shown to contribute to the positive regulation of TAG accumulation in response to N deficiency; they encode a monogalactosyldiacylglycerol (MGDG)-specific lipase, a putative transcriptional factor, and a PDAT, respectively. Additionally, ADP-Glc pyrophosphorylase (Li et al., 2010; Blaby et al., 2013) and isoamylase (Work et al., 2010) have been reported to affect TAG accumulation negatively in N-deficient conditions. Recently, targeted disruption of the gene encoding a UDP-Glc pyrophosphorylase in a diatom *Phaeodactylum tricornutum* by using meganucleases and transcription

[1] This work was supported by the Japan Society for the Promotion of Science (Grant-in-Aid for Scientific Research nos. 25850068 to Ma.K. and 25120714 to H.F.), the Advanced Low Carbon Technology Research and Development Program of the Japan Science and Technology Agency (Mi.K. and H.F.), and the Core Research for Evolutional Science and Technology Program of the JST (N.S.).

[2] Present address: Faculty of Bioscience and Applied Chemistry, Hosei University, Tokyo 184–8584, Japan.

* Address correspondence to fukuzawa@lif.kyoto-u.ac.jp.

The author responsible for distribution of materials integral to the findings presented in this article in accordance with the policy described in the Instructions for Authors (www.plantphysiol.org) is: Hideya Fukuzawa (fukuzawa@lif.kyoto-u.ac.jp).

Ma.K. and H.F. designed the research and wrote the article; Ma.K., Y.S., H.S., T.Y., A.A., Mi.K., M.H., N.S., and H.F. performed the research; T.Y. performed the data processing for RNA sequencing.

[OPEN] Articles can be viewed without a subscription.

www.plantphysiol.org/cgi/doi/10.1104/pp.15.00319

activator-like effector nucleases led to 3-fold higher levels of TAG accumulation than that in the wild type in N deficiency (Daboussi et al., 2014), suggesting that genetic modification could enhance lipid accumulation in microalgal cells.

Previously identified factors affecting the levels of TAG accumulation, the transcription factor NRR1, and metabolic enzymes PGD1, PDAT1, ADP-Glc pyrophosphorylase, and isoamylase were reported by characterizing mutants with aberrant TAG accumulation in N-deficient conditions, but no regulatory factors involved in protein modification leading to global changes in gene expression in different stress conditions (i.e. N/S deficiency) have been reported.

In the model plant Arabidopsis (*Arabidopsis thaliana*), two calcineurin B-like interacting protein kinases (CIPKs), CIPK23 (Ho et al., 2009) and CIPK8 (Hu et al., 2009), have been reported to function in a nitrate-sensing mechanism. Similarly, other kinases might function in microalgal nutrient-deficient response mechanisms. Dual-specificity Tyr phosphorylation-regulated kinases (DYRKs) have been reported to regulate cell division and growth in many eukaryotes (Aranda et al., 2011). In budding yeast (*Saccharomyces cerevisiae*), the DYRK family gene Yet another kinase1 (Yak1) is well characterized as a negative regulator of cell division in Glc-deficient conditions, antagonizing Rat Sarcoma/cAMP and target of rapamycin signaling (Aranda et al., 2011). Human DYRK1A, which has been studied extensively, was discovered as a gene product localized in the Down syndrome-critical region on chromosome 21 (Guimerá et al., 1996). DYRKs autophosphorylate a critical Tyr in their activation loop, but they function only as Ser/Thr kinases against their substrates (Yoshida, 2008). Downstream effects mediated by substrates of DYRKs include increased activity of transcription factors, modulation of subcellular protein localization, and regulation of enzyme activity (Aranda et al., 2011; Becker, 2012). One characteristic feature of several DYRKs is their function as priming kinases, in which phosphorylation of given residues by a DYRK is a prerequisite for the subsequent phosphorylation of a different residue by another protein kinase, such as glycogen synthase kinase3 or polo-like kinase (Aranda et al., 2011). In photosynthetic eukaryotes, however, there have been no reports on the physiological functions of DYRK proteins. In this report, we present evidence showing that a DYRK has pleiotropic effects on metabolic processes, including accumulation of TAG, regulation of cell division, and photosynthesis.

RESULTS

Fluorescence-Activated Cell Sorting-Based Screening of Low TAG-Accumulating Mutants in Nutrient-Deficient Conditions

To isolate regulatory mutants with low-TAG accumulation during S deficiency, a tagged mutant pool was constructed by using a PCR-amplified DNA fragment encoding the hygromycin resistance gene *aminoglycoside phosphotransferaseVII* (*aphVII*) to transform a wild-type C-9 strain of green alga as described previously (Wang et al., 2014). In total, 8,000 hygromycin-resistant colonies cultured in Tris-acetate phosphate medium without an S source (TAP − S) to induce TAG accumulation were stained using a fluorescent dye, boron dipyrromethene (BODIPY), and subjected to cell sorting by fluorescence-activated cell sorting (FACS; Fig. 1A). A group of cells showing the same levels of fluorescence intensity during S deficiency as those of the parental wild-type strain in S-replete conditions (Fig. 1B) was collected. To concentrate cells showing a lower level of TAG accumulation, the sorted cells were rescreened by FACS in the same S-deficient conditions. The collected cell mixture was spread on Tris-acetate phosphate (TAP) agar plates; 188 individual colonies appeared on the TAP plates and were cultured individually for 2 d. By using a fluorescent dye, AdipoRed, as an indicator of TAG accumulation, the cell line with the weakest fluorescence was selected and designated as *triacylglycerol accumulation regulator1-1* (*tar1-1*) for additional analyses. To evaluate the accumulation of TAG in *tar1-1*, the fluorescence patterns of chlorophyll content were compared with those of wild-type cells. After 2 d of S deficiency, the fluorescence level in *tar1-1* cells was lower than that in wild-type cells (Fig. 1C).

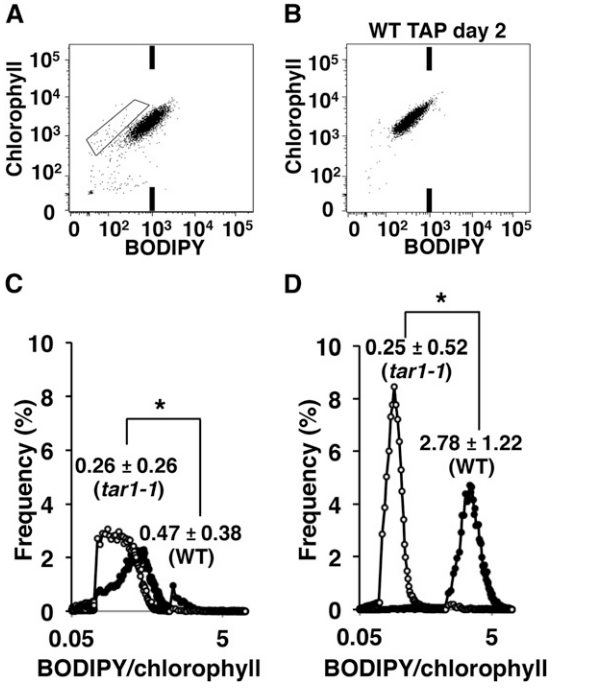

Figure 1. FACS and flow cytometric analyses of a *C. reinhardtii* mutant. A, Dot blot of the mixture of transformed cells incubated for 2 d in TAP − S medium. The box denotes the sorting gate used for isolation of mutants with a low level of relative fluorescence intensities corresponding to the fraction in which parental wild-type cells cultured in normal TAP medium (B). Histogram showing distribution of BODIPY fluorescence intensity normalized by chlorophyll autofluorescence per cell of the wild type (black circles) and *tar1-1* (white circles) in S-deficient (C) and N-deficient (D) conditions. Mean values ± SD from three biological replicates are shown. WT, Wild type; *, significant difference ($P < 0.01$) from the wild type by Student's *t* test.

Lipid Droplets Were Not Well Developed in *tar1-1* Mutant in S- and N-Deficient Conditions

Additionally, during S deficiency, in N-deficient conditions, *tar1-1* cells showed lower levels of BODIPY fluorescence than those in wild-type cells (Fig. 1D). In the histogram of BODIPY to chlorophyll ratios per cells, the population shift in *tar1-1* versus the wild type during N deficiency was observed to be more pronounced than that observed during S deficiency (Fig. 1, C and D). Lipid droplets (LDs), which mainly consist of neutral lipid TAG, were visualized using a confocal microscope after staining with AdipoRed. In contrast to the fact that LDs were abundant and well developed in wild-type cells cultured for 2 d in S- and N-deficient conditions (Fig. 2A), LDs were less abundant and smaller in *tar1-1* cells. Two complementation lines of *tar1-1*, named C1 and C2, described in the section below showed restored levels of LD accumulation. In N-deficient conditions, the average numbers of LDs in *tar1-1* and wild-type cells were 6.8 and 11.8, respectively (Supplemental Fig. S1A). The average diameters of LDs in *tar1-1* and wild-type cells were 361.7 and 663.1 nm, respectively (Supplemental Fig. S1B). When we compared sectional images of wild-type and *tar1-1* cells in N-deficient conditions, larger LDs were developed in wild-type cells than in *tar1-1* cells, but starch granules were present in both cell lines (Fig. 2B). These results indicated that the gene responsible in *tar1-1* cells regulates the induction of TAG accumulation positively in both N- and S-deficient conditions.

Molecular Characterization of the *tar1-1* Mutant

To identify the introduced tag insertion site in the *tar1-1* mutant, thermal asymmetric interlaced PCR was performed. Random primers and DNA tag-specific primers generated the DNA tag sequence fused to the 5′-untranslated region sequence (position: −548 nucleotides) of the gene locus *Cre08.g381950* on chromosome 8 (Merchant et al., 2007; Fig. 3A). The sequences of the *TAR1* complementary DNA (cDNA) and genomic DNA in green alga strain C-9 strain were determined by 5′- and 3′-RACE and genomic PCR using a fosmid clone, GCRFno11_b05, which spanned the *TAR1* gene locus. Gene structure based on the sequencing of cDNAs and

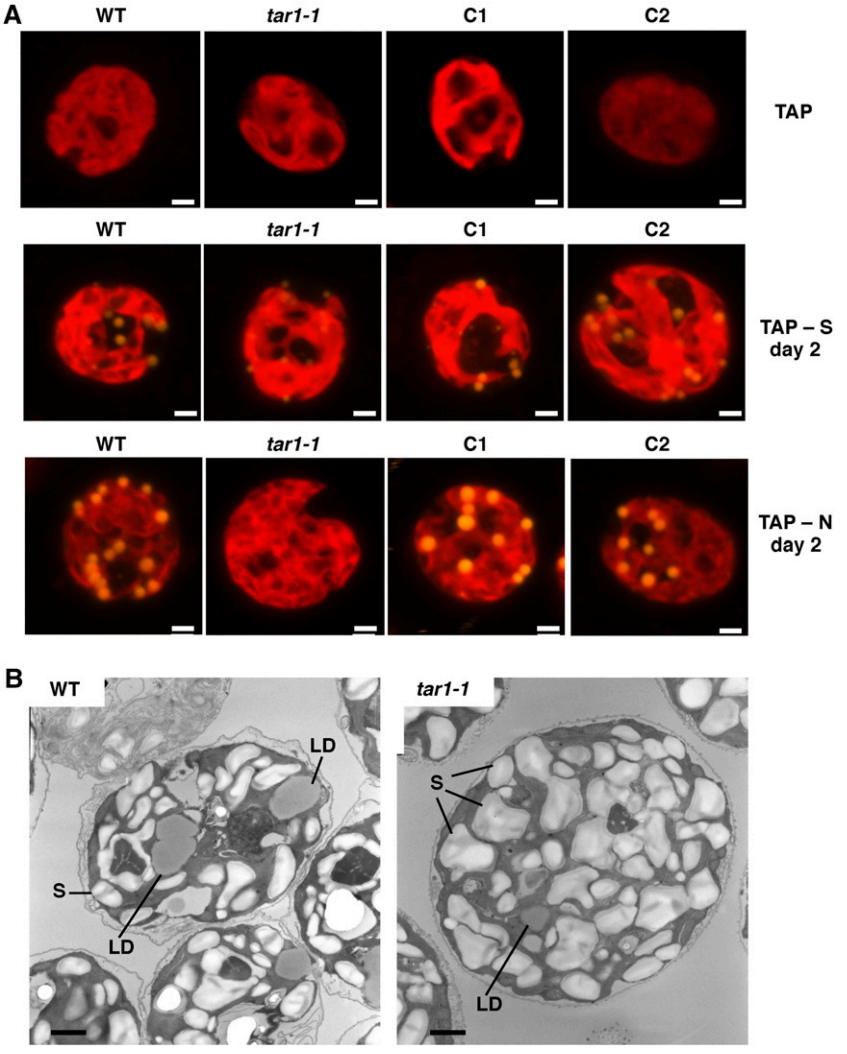

Figure 2. Development of LDs in wild-type, *tar1-1*, and complementation lines (C1 and C2) in S- and N-deficient conditions (TAP − S and TAP − N, respectively) for 2 d substituted from nitrogen-replete conditions (TAP). A, Fluorescence images were recorded using a laser-scanning confocal microscope. LDs were visualized by staining with AdipoRed. Bars = 2 μm. B, Transmission electron microscopic images of wild-type and *tar1-1* cells 2 d after transfer to N-deficient conditions. Bars = 1 μm. S, Starch granule; WT, wild type.

genomic DNA clones from the C-9 strain was identical to that predicted by a *C. reinhardtii* gene annotation: Augustus update 10.2 (based on the JGI version 4 genome in Phytozome; http://phytozome.jgi.doe.gov/pz/portal.html#!info?alias=Org_Creinhardtii). We designated this gene TAR1 based on the functional analysis described below. The gene product of TAR1 has a kinase domain (Fig. 3A; Supplemental Fig. S2), and amino acid residues 495 to 830 showed 47% sequence identity with that of budding yeast Yak1, a negative regulator of cell proliferation in nutritional stress conditions (Aranda et al., 2011). The kinase domain of TAR1 also has conserved functional features of the DYRK family, such as an ATP anchor, a phosphate anchor, a catalytic loop, a cation-binding site, and an activation loop (Supplemental Fig. S2B). The mRNA expression level of *TAR1* did not change in response to N deficiency, and its expression was not detected in the *tar1-1* mutant in S- or N-deficient conditions (Fig. 3, B and C).

To verify the relationship between *TAR1* and the *tar1-1* phenotype, we examined the genetic linkage of the DNA tag insertion in the *TAR1* locus to the low-TAG accumulation phenotype in N-deficient conditions (Supplemental Fig. S3). The *tar1-1* mutant (mt^-) was crossed with a wild-type strain CC-125 (mt^+) two times. Six sets of tetrads were obtained from the second cross.

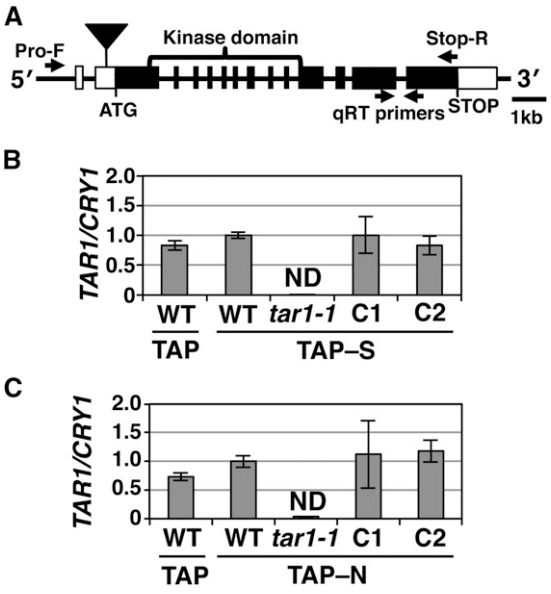

Figure 3. Structure and expression of the *TAR1* gene. A, The *TAR1* gene contains 14 exons (thick boxes) separated by 13 introns. The insertion site of the DNA cassette encoding the hygromycin resistance gene (*aphVII*) in *tar1-1* is indicated by a black triangle. The region encoding the kinase domain is indicated. Positions of primers used for amplification of DNA fragments for the region for complementation (Pro-F and Stop-R) and those used for qRT-PCR are indicated. qRT-PCR analyses of *TAR1* in wild-type, *tar1-1*, and two complementation lines (C1 and C2) cultured for 6 h in S-deficient (TAP − S) or S-replete conditions (TAP for the wild type; B) or N-deficient (TAP − N) or N-replete (TAP for the wild type) conditions (C). Expression of *TAR1* was normalized to *CRY1*. Data indicate mean value ± SD from three biological replicates. Supplemental Table S6 shows primer sequences. ND, Not detected; WT, wild type.

The mutant phenotype with low levels of AdipoRed fluorescence segregated in a 2:2 ratio in all of the six tetrads (Supplemental Fig. S3A). All of the progeny with the mutant phenotype had the DNA tag insertion in the *TAR1* gene (Supplemental Fig. S3B) and showed hygromycin resistance (Supplemental Fig. S3C). Thus, the DNA tag insertion in *tar1-1* seemed to be closely linked to the mutation causing the low-TAG phenotype.

To confirm that the described phenotypes were caused by a mutation of the *TAR1* gene, a genomic PCR fragment containing 13.2 kb of the wild-type *TAR1* coding region containing the promoter region (approximately 1 kb upstream of the 5′-untranslated region) was cloned into the expression vector pGenD-HA harboring a paromomycin resistance gene cassette. The resultant plasmid, pGenD-TAR1, was used to transform the *tar1-1* mutant, and the obtained transformants were selected on TAP agar medium containing 10 mg L^{-1} of paromomycin and further screened by genomic PCR with gene-specific primers. In 2 of 24 PCR-positive lines (C1 and C2) harboring the wild-type *TAR1* gene, the low-TAG accumulation phenotypes were restored (Fig. 4A; Supplemental Fig. S4A), including expression of the *TAR1* gene (Fig. 3, B and C). This low rate of frequency for complementation of the *tar1-1* mutation might be caused by partial insertion of the long genomic DNA fragment of 13.2 kb encoding the *TAR1* gene. These results strongly suggested that the phenotypes of *tar1-1* related to TAG were caused by disruption of the *TAR1* gene.

Phosphorylation Activity of the DYRK Domain in TAR1

To test whether TAR1 has phosphorylation activity, a partial triacylglycerol accumulation regulator1 (pTAR1) protein (Thr-421 to Leu-859) containing the kinase domain (Val-495 to Ile-830; Supplemental Fig. S2) was cloned into a pCold TF vector and expressed in *Escherichia coli*. We tested the phosphorylation activities of wild-type pTAR1 and a kinase-dead (KD) mutant, $pTAR1^{KD}$, with a K523R substitution at the putative phosphate anchor site according to the report on yeast Yak1 (Martin et al., 2004; Supplemental Fig. S2). An in vitro assay using [γ-^{32}P]ATP revealed that 52-kD pTAR1 had auto- and transphosphorylation activities with casein and myelin basic protein (MBP) but did not show any activity with histone (Fig. 5). $pTAR1^{KD}$ did not show any phosphorylation activity, confirming that Lys-523 is essential for kinase activity. Additional phosphorylated bands observed at approximately 45 kD could be generated by processing of the 52-kD pTAR1. Without magnesium in the assay reactions, no phosphorylation activity against pTAR1 itself, casein, or MBP proteins was detected, suggesting that Mg^{2+} is necessary for pTAR1 activity (Fig. 5).

The *tar1-1* Mutant Showed Low-TAG Accumulation in S- and N-Deficient Conditions

To evaluate the influence of disruption of the *TAR1* gene on the accumulation of carbon metabolites, the

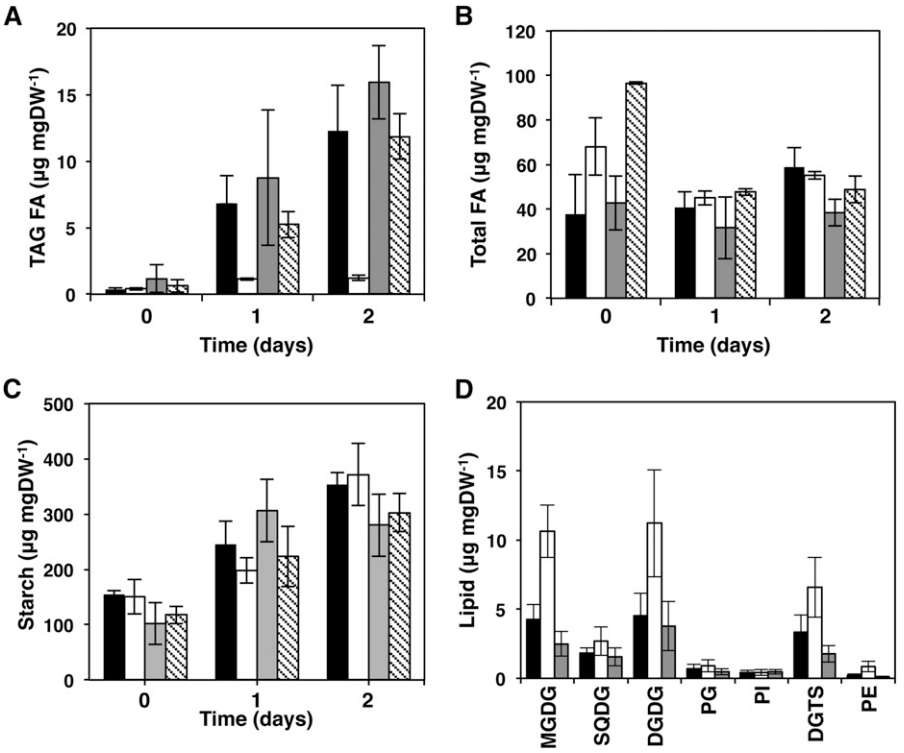

Figure 4. Levels of lipids and starch in N-deficient conditions. Cells were collected every 24 h for 2 d after changing culture medium to TAP − N. Amounts of total fatty acids in TAG (A), total fatty acids in total lipids (B), and starch (C) normalized by cell weight were measured in the wild type (black bars), *tar1-1* (white bars), C1 (gray bars), and C2 (striped bars). D, Amount of major polar lipid classes normalized dry cell weight in the wild type, *tar1-1*, and C1 cells after culturing for 2 d in TAP − N medium. Data in all experiments indicate means value ± SD from three biological replicates. DGTS, Diacylglycerol-*N*,*N*,*N*-trimethylhomo-Ser; DW, dry weight; FA, fatty acids; PE, phosphatidylethanolamine; PG, phosphatidylglycerol, PI, phosphatidylinositol; SQDG, sulfoquinovosyldiacylglycerol; WT, wild type.

amounts of lipid and starch were quantified in S- and N-deficient conditions. The amount of TAG in *tar1-1* was 1.87 μg mg^{-1} dry weight, which corresponded to 52% of that in wild-type cells (3.61 μg mg^{-1} dry weight) after 2 d of S deficiency (Supplemental Fig. S4A). However, the amounts of total fatty acids and starch did not differ significantly between *tar1-1* and the wild type in S-deficient conditions (Supplemental Fig. S4, B and C).

In N-deficient conditions, the amount of TAG in *tar1-1* was 1.23 μg mg^{-1} dry weight, which corresponded to 10% of that (12.3 μg mg^{-1} dry weight) in wild-type cells after 2 d (Fig. 4A). Similar to S-deficient conditions, the amounts of total fatty acids and starch did not differ significantly between *tar1-1* and wild-type cells in N-deficient conditions (Fig. 4, B and C). In *tar1-1* cells, TAG accumulation was severely impaired during N deficiency compared with that during S deficiency (Fig. 4A; Supplemental Fig. S4A). Detailed analyses of the cellular lipid composition revealed that the amounts of plastidial membrane lipids (such as MGDG, 10.6 μg mg^{-1} dry weight; digalactosyldiacylglycerol [DGDG], 11.2 μg mg^{-1} dry weight) in *tar1-1* cells in N-deficient conditions were 2.5-fold larger than those (MGDG, 4.2 μg mg^{-1} dry weight; DGDG, 4.5 μg mg^{-1} dry weight) in wild-type cells in the same conditions (Fig. 4D). The increase in major plastidial lipids MGDG and DGDG was achieved through total glycerolipids instead of TAG accumulation in *tar1-1*. In the C1 line, these metabolic phenotypes o the parental wild-type strain were restored (Fig. 4, A and D; Supplemental Fig. S4A).

Physiological Phenotypes of *tar1-1* Cells

To examine the physiological phenotype of the *tar1-1* mutant, time-course changes in the amount of chlorophyll (Supplemental Fig. S5A), maximum photosynthetic oxygen (O_2)-evolving rate (Supplemental Fig. S5B), acetate concentration in the medium (Supplemental Fig. S5C), cell dry weight (Supplemental Fig. S5D), cell size (Supplemental Fig. S5E), cell numbers (Supplemental Fig. S5F), and cell survival rate based on Evans Blue staining (Supplemental Fig. S6A) were measured in S-deficient conditions. It was found that all time-dependent changes in these phenotypes did not differ significantly between *tar1-1* and wild-type cells.

However, a notable phenotype of the *tar1-1* mutant was the retarded degradation of chlorophyll (Fig. 6A), which resulted in a stay-green phenotype in culture (Fig. 6B), in N-deficient conditions. In contrast, parental wild-type cells showed chlorosis in these conditions. The large subunit of Rubisco (rbcL) and cytochrome *f* are rapidly degraded in N-deficient conditions (Wei et al., 2014). In contrast, *tar1-1* cells maintained higher levels of these proteins in the same conditions (Fig. 6C). The maximum rate of photosynthetic O_2 evolution (V_{max}) decreased rapidly in wild-type cells during a 2-d culture in N-deficient conditions (from 238.7–17.3 μmol O_2 mg chlorophyll^{-1} h^{-1}; Fig. 6D). However, *tar1-1* cells retained their photosynthetic activity in N-deficient conditions (from 226.9–81.4 μmol O_2 mg chlorophyll^{-1} h^{-1}; Fig. 6D). The residual acetate concentration in the medium of the *tar1-1* culture (0.16 mg mL^{-1}) was 8-fold higher than that of wild-type

cultures (0.02 mg mL^{-1}) after 2 d of growth in N-deficient conditions (Fig. 6E). For *tar1-1* cells, cell dry weight per milliliter of culture was not different from that of wild-type cells (Fig. 6F), but the cell volume of *tar1-1* cells was 20% larger than that of wild-type cells after 2 d of growth in N-deficient conditions (Fig. 6G). Cell number in the *tar1-1* culture did not change as a result of N deficiency, whereas that in the wild-type culture increased, even in N-deficient conditions (Fig. 6H). The growth rates of *tar1-1* and wild-type cells in N-replete conditions were similar (Supplemental Fig. S7). The cell viability of the *tar1-1* mutant was not significantly different from that of the wild type after 6 d of N deficiency (Supplemental Fig. S6B). In the C1 line, all of these physiological phenotypes of the parental wild-type strain were restored in N-deficient conditions (Fig. 6).

These results suggested that TAR1 enhances the degradation of chlorophyll and photosynthesis-related proteins, which leads to a decrease of photosynthetic activity in wild-type cells in N-deficient conditions. TAR1 also might enhance acetate assimilation and rate of cell division and prevent increase of cell biomass.

Differentially Expressed Genes in the *tar1-1* Mutant in N-Deficient Conditions

Various metabolic and physiological phenotypes of *tar1-1* during N deficiency suggested that disruption of the *TAR1* gene led to a global change in gene expression. To find genes with expression that was affected by TAR1, differentially expressed genes (DEGs) between N-deficient and -replete conditions in each of the *tar1-1*,

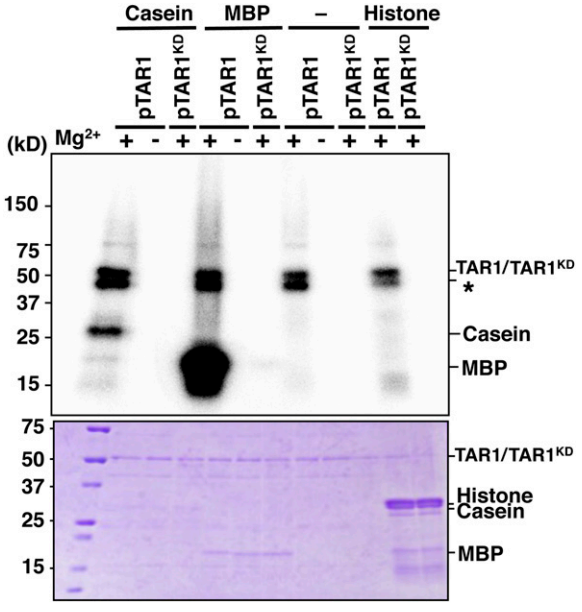

Figure 5. In vitro kinase assay using pTAR1. A pTAR1-containing kinase domain and that of a K523R substitution of the putative phosphate anchor Lys (pTAR1^{KD}) were incubated with [γ-^{32}P]ATP in the presence or absence of Mg^{2+}. Proteins are stained with Coomassie Brilliant Blue in lower. *, Putative processed product of pTAR1.

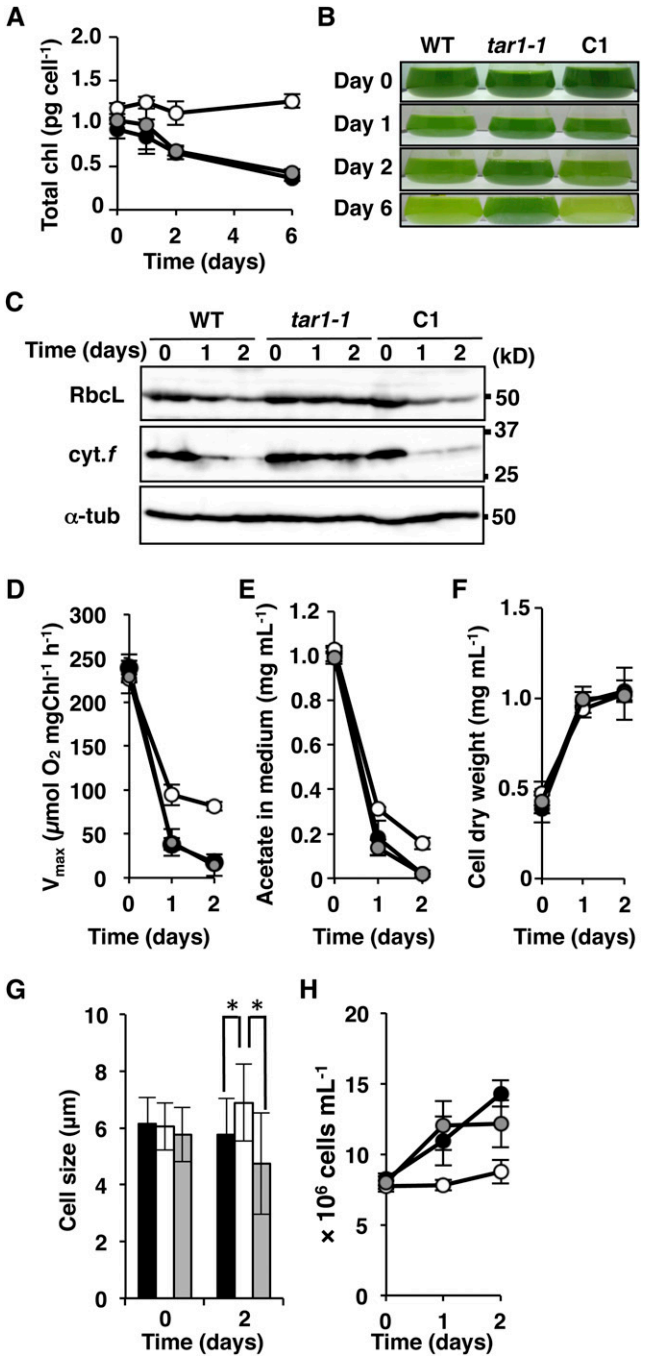

Figure 6. Phenotypic changes of the wild type (black), *tar1-1* (white), and C1 (gray) after transfer to N-deficient conditions. A, Chlorophyll contents. B, Images of cultures. C, Immunoblot analysis using antibodies against rbcL, cytochrome *f*, and α-tubulin. D, Maximum photosynthetic rates of O_2 evolution (V_{max}). E, Extracellular acetate concentration. F, Cell dry weight. G, Averaged cell diameter of wild-type and *tar1-1* cells in N-replete conditions and after N deficiency for 2 d. *, Significant difference ($P < 0.01$) from the wild type and C1, respectively, by Student's *t* test. H, Cell numbers. Data in all experiments indicate mean values ± SD from three biological replicates. α-tub, α-Tubulin; Chl, chlorophyll; cyt. *f*, cytochrome *f*; WT, wild type.

wild-type, and C1 lines were estimated by the DESeq algorithm with a *q*-value cutoff of less than 0.05 from RNA sequencing (RNA-seq) data (Supplemental Table S1; Supplemental Data Set S1). For RNA-seq analysis, RNA was extract from each line 6 h after being transferred to Tris-acetate phosphate medium without a nitrogen source (TAP − N; normal TAP medium as a control), because the previous reports revealed that TAG accumulation starts in the cells (Park et al., 2015); expression of a large part of conserved N-regulated genes has already responded (Schmollinger et al., 2014) at that time point. Consequently, the expression levels of 937, 509, and 405 genes were increased significantly in N-deficient conditions in *tar1-1*, wild-type, and C1 cells, respectively (Fig. 7A). Conversely, the expression levels of 1,255, 1,155, and 775 genes were decreased significantly in N-deficient conditions in *tar1-1*, wild-type, and C1 cells, respectively (Fig. 7B). Some representative N-regulated genes, such as *Ammonium transporter4* and *NRR1*, reported by Schmollinger et al. (2014) were included in the DEGs in wild-type cells (Supplemental Data Set S1).

In these DEGs in N-deficient conditions, 153 genes were up-regulated in both wild-type and C1 but not *tar1-1* cells (group a), 703 genes were up-regulated in *tar1-1* but not wild-type and C1 cells (group b), and 119 genes were up-regulated in all lines (group c; Fig. 7A). Conversely, 146 genes were down-regulated in both wild-type and C1 but not *tar1-1* cells (group d), 450 genes were down-regulated in the *tar1-1* line but not wild-type and C1 cells (group e), and 527 genes were down-regulated in all lines (group f; Fig. 7B). The largest number of genes belonged to group b. Genes in each group are listed in Supplemental Data Sets S2 to S7.

To focus on genes with expression that was affected strongly by disruption of the *TAR1* gene in *tar1-1*, DEGs between wild-type and *tar1-1* cells in N-deficient conditions and non-DEGs between wild-type and C1 cells in N-deficient conditions were selected in Supplemental Tables S2 to S4 from genes in groups a, b, and f, respectively. Eight genes, including *Argininosuccinate synthetase1* (*AGS1*), *Formamidase/acetamidase1* (*AMI1*), *Degradation of Urea1* (*DUR1*), *Carbamoyl phosphate synthase, large subunit1* (*CMPL1*), *Argininosuccinate lyase7* (*ARG7*), *Acetylglutamate kinase1* (*AGK1*), *Ornithine carbamoyltransferase1* (*OTC1*), and *Degradation of Urea2* (*DUR2*), involved in N assimilation were included in Supplemental Table S2, implying defective responses to N deficiency in *tar1-1* cells; 2 *Vesicle-Inducing Protein in Plasmids* (*VIPP*) genes involved in thylakoid maintenance are included in Supplemental Table S3, and 11 genes in tetrapyrrole biosynthesis are included in Supplemental Table S4. These changes in gene expression were consistent with the stay-green phenotype of *tar1-1* during N deficiency.

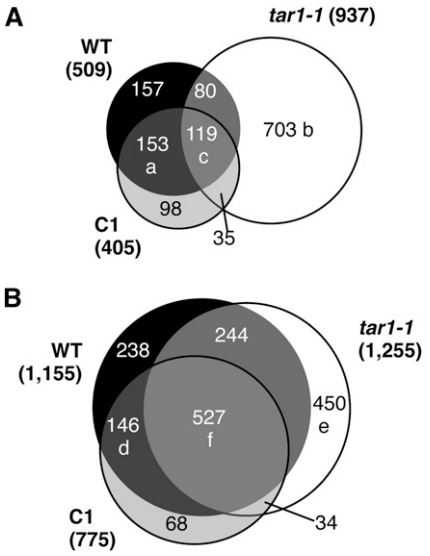

Figure 7. Venn diagram showing genes differentially expressed in the wild type, *tar1-1*, and C1 at 6 h after N-deficient conditions compared with N-replete conditions. Numbers of DEGs in each strain are shown in parentheses. A, Genes with expression that was up-regulated in N-deficient conditions in both the wild type and C1 but not *tar1-1* (group a), only in *tar1-1* but not in the wild type and C1 (group b), and in all lines (group c). B, Genes with expression that was down-regulated in N-deficient conditions in both the wild type and C1 but not *tar1-1* (group d), only in *tar1-1* but not in the wild type and C1 (group e), and in all lines (group f). WT, Wild type.

DISCUSSION

In the *tar1-1* mutant, the amount of TAG declined by 52% and 10% compared with wild-type cells after a 2-d culture with S- and N-deficient conditions, respectively (Fig. 4A; Supplemental Fig. S4A). The level of TAG accumulation in *tar1-1* cells during N deficiency was the lowest compared with that in previously isolated low-TAG accumulation mutants *nrr1-1* (52% of the wild type; Boyle et al., 2012), *pgd1* (50% of the wild type; Li et al., 2012), and *pdat1-RNA interference* (72% of the wild type; Yoon et al., 2012), suggesting that TAR1 functions as a critical positive regulator in wild-type cells in N-deficient conditions. So far, no mutants with a low-TAG accumulation phenotype in S-deficient conditions have been reported. Our results suggested that TAR1 regulates the levels of TAG during not only N deficiency but also, S deficiency. Consumption of acetate in the culture medium by *tar1-1* cells was slower than that by the wild type (Fig. 6E), implying that acetate supply required for de novo synthesis of TAG was defective in *tar1-1* mutant. Unexpectedly, the expression levels of genes involved in acetate and TAG metabolism, such as *Acetate Kinase1*, *Aspartate Kinase2*, and *Acetyl-CoA synthetase1-3* for acetate assimilation (Spalding, 2009) and *PGD1*, *NRR1*, *PDAT1*, and other diacylglycerol acyltransferase genes for TAG synthesis (Riekhof and Benning, 2009), were not strongly affected by *TAR1* mutation despite the low-TAG accumulation phenotype in *tar1-1* during N deficiency. The following two possibilities are considered: (1) some of these genes might be regulated post-transcriptionally by TAR1, or (2) their expression levels in *tar1-1* might be different from those in the wild type at

earlier or later stages during N deficiency than the sampling time in this study. In contrast to TAG accumulation, the *tar1* mutation did not have any influence on starch content during the first 2 d in N deficiency, suggesting that TAR1 is not involved in N deficiency-inductive starch accumulation. However, we should mention that a conversion of starch into lipids might occur in microalgal cells at the late stage of N deficiency (Bellou and Aggelis, 2012). Additional investigation of starch and lipid metabolisms in wild-type and *tar1-1* cells at the later stage of N deficiency is necessary to reveal the function of the *TAR1* gene in the conversion mechanism.

Chlorosis and protein degradation observed in N-deficient wild-type cells are supposed to be caused by the recycling of N (Schmollinger et al., 2014) and be used for protection against overreduction of the photosynthetic electron transport chain in N-deficient conditions (Li et al., 2012). TAG accumulation is supposed to protect cells against oxidative damage in N-deficient conditions, because de novo fatty acid synthesis for TAG accumulation can consume a part of the accumulated NADPH derived from photosynthesis (Johnson and Alric, 2013). However, the *tar1-1* mutant maintained cell viability similar to wild-type cells during N deficiency, although it showed low levels of TAG accumulation, and maintained chlorophyll, photosynthesis-related proteins, and photosynthetic activity. Therefore, *tar1-1* is likely to avoid oxidative damage by a 2.5-fold larger accumulation of plastidial membrane lipids MGDG and DGDG compared with that in wild-type cells during N deficiency.

Expression of genes involved in thylakoid maintenance and stress resistance was significantly increased in *tar1-1* but not wild-type cells (Supplemental Table S3). For example, the *VIPP1* and *VIPP2* genes are essential for the maintenance of thylakoids in green alga (Nordhues et al., 2012) and Arabidopsis (Kroll et al., 2001). *Pyridine nucleotide-disulphide oxidoreductase1* encodes a protein with 23.9% similarity to Arabidopsis membrane-bound monodehydroascorbate reductase3, which has overexpression that increases protection against oxidative stress (Wang et al., 1999). Increase of these genes' expressions in the *tar1-1* during N deficiency might contribute to maintaining cell viability at a wild type-like level. The expression levels of

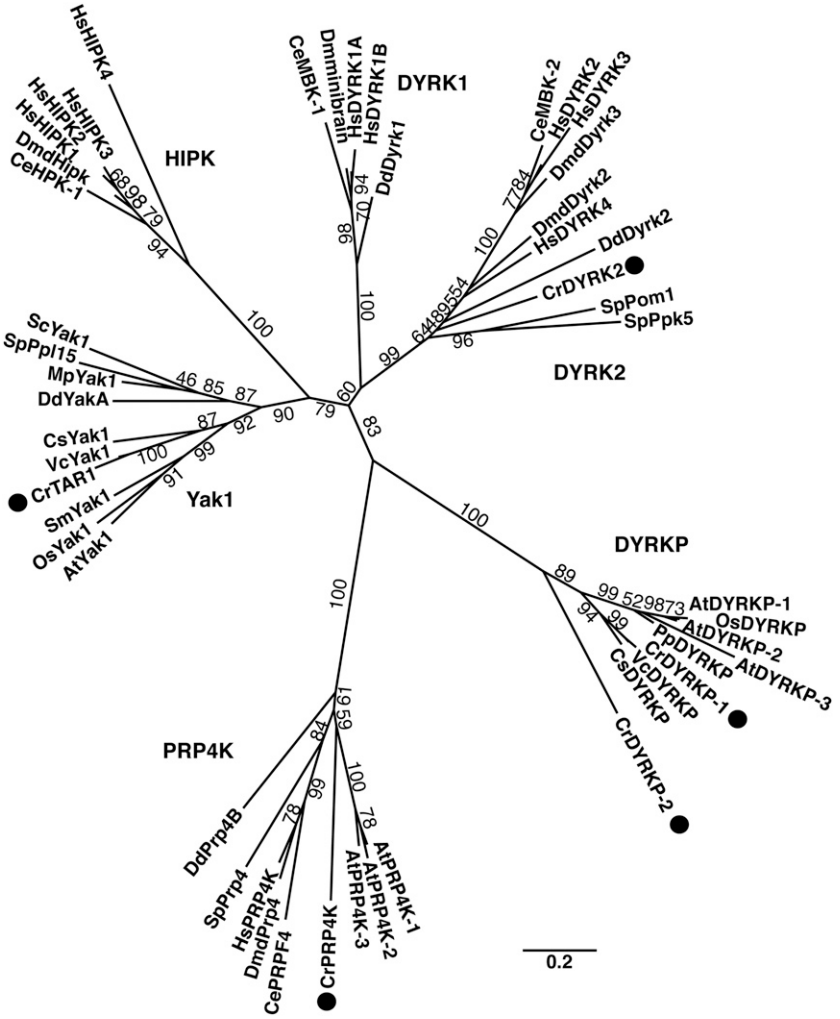

Figure 8. Phylogenetic tree of TAR1 and related DYRKs constructed by comparing amino acid sequences of the kinase domains. The DYRK family (Aranda et al., 2011) consists of six subgroups: Yak1, DYRK1, DYRK2, DYRKP, PRP4K, and HIPK. The Yak1 subgroup consists of fungal (ScYak1, DdYakA, SpPpk15, and MpYak1), land plant (SmYak1, AtYak1, and OsYak1), and algal (CrTAR1, VcYak1, and CsYak1) clades. DYRKP is a plant-specific subgroup. *C. reinhardtii* proteins belonging to each DYRK subgroup are marked by black circles. The tree was generated using TreeFinder (Jobb et al., 2004) using the maximum likelihood algorithm. Bootstrap values (1,000 replicates) are indicated at branch nodes, and the scale bar indicates the number of amino acid substitutions per site. Supplemental Table S5 shows accession numbers of each protein sequence.

Glutamate1-semialdehyde (*GSA*), *Mg-protoporphyrin O-methyltransferase* (*CHLM*), *Uroporphyrinogen-III decarboxylas* (*HEME*), *Uroporphyrinogen-III synthase* (*UROS*), *Protoporphyrinogen oxidase1* (*PPX1*), *Mg-protoporphyrin IX monomethyl ester* (*oxidative*) *cyclase 1A* (*CTH1A*), *Mg-chelatase I subunit1-1* (*CHLI1*), *Mg-chelatase subunit H1* (*CHLH1*), *Chlorophyll synthase* (*CHLG*), *Mg-chelatase I subunit1-2* (*CHLI2*), and *Glutamyl/glutaminyl-tRNA synthetase* (*GTS2*) involved in tetrapyrrole biosynthesis (Schmollinger et al., 2014) in *tar1-1* were 5-fold or more higher than those in wild-type cells in N-deficient conditions (Supplemental Table S4), suggesting that tetrapyrrole biosynthesis was still active to maintain chlorophyll content and photosynthetic activity in *tar1-1* compared with wild-type cells.

Although wild-type cells almost doubled in number after 2 d in N-deficient conditions, as reported previously (Schmollinger et al., 2014), the cell numbers of *tar1-1* did not increase in these conditions (Fig. 6H), suggesting that the *tar1* mutation leads to hypersensitivity of the cell division response to N-deficient conditions. Increases in cell volume and the amounts of membrane lipids in *tar1-1* cells could be partially attributed to the inhibition of cell division after transfer to N-deficient conditions, whereas the cell volume of wild-type cells was kept constant (Fig. 6G). Additional analyses of the effects of the *tar1* mutation on the cell cycle by using synchronized culture cells would reveal the precise function of TAR1 in cell division during N deficiency.

C. reinhardtii TAR1 was shown to belong to the Yak1 subgroup of the DYRK family. This kinase family consists of a total six subgroups: Yak1, DYRK1, DYRK2, PremRNA-processing factor4 kinase (PRP4K), Homeodomain interacting protein kinase (HIPK), and the newly assigned plant-specific DYRK (DYRKP; Fig. 8). Based on BLAST searches using the kinase domain sequence of TAR1 as the query, putative DYRK homolog genes were found from land plants and algal genome databases (Supplemental Table S5), and their kinase domain sequences were grouped separately from five previously assigned DYRK subgroups. Therefore, we named this plant-specific subgroup DYRKP. In addition to *TAR1*, four putative green alga DYRK genes belonging to the DYRKP, DYRK2, and PRP4K subgroups were detected in the green alga genome database (Fig. 8). In the Yak1 subgroup, including fungus, algal, and plant orthologs, only yeast Yak1 has been characterized as a negative regulator of cell division in Glc-deficient conditions (Moriya et al., 2001). Both algal TAR1 and yeast Yak1 are involved in nutrient deficiency-responsive signals and the regulation of cell division. Yak1 was shown to phosphorylate transcription factors, such as Heat shock transcription factor1, Multicopy suppressor of SFN1 mutation2, and PGK promoter directed over production (Pop2), and transduce the Glc-limiting stress signal into the transcriptional control of genes involved in the cell cycle (Lee et al., 2008). In green alga, *C. reinhardtii* Chromatin assembly factor1 (CrCaf1), with 36% sequence identity with yeast Pop2, was reported to function as a deadenylase-degrading poly(A) (Zhang et al., 2013). Because the kinase domain of TAR1 had auto- and transphosphorylation activities in the presence of magnesium (Fig. 5), the CrCAF1 protein is one of the candidate substrates for TAR1-mediated phosphorylation. Other candidates could be revealed by phosphoproteomics analysis by comparing the numbers and types of phosphorylated peptides detected from *tar1-1* and wild-type cells in nutrient-deficient and -replete conditions.

Induction of expression of N assimilation-related genes in green alga cells was impaired in *tar1-1* (Supplemental Table S2). These genes are classified into two groups: (1) genes for organic nitrogen transport and use, such as *AMI1* encoding putative formamidase/acetoamidase and *DUR1* and *DUR2* encoding putative urea carboxylase and allophanate lyase, respectively (Fernández et al., 2009), and (2) genes for Arg synthesis from Glu, including *AGS1*, *CMPL1*, *ARG7*, *AGK1*, and *OTC1* (Vallon and Spalding, 2009). These results suggest that TAR1 may be involved in organic nitrogen transport and Arg biosynthesis during N deficiency by modulating the expression of these genes.

Based on characterization of phenotypes of the *tar1-1* mutant, TAR1 has pleiotropic functions during N deficiency (Fig. 9), possibly by means of phosphorylation-mediated activation or repression of putative transcription factors. However, because most of the phenotypes in *tar1-1* during S deficiency were like the wild type, except for TAG accumulation, the function of TAR1 may be restricted to regulation of lipid metabolism in S-deficient conditions. Identification of phosphorylation substrates for TAR1 would provide unique insights to understand the roles of DYRKs in photosynthetic eukaryotes and nutrient-sensing mechanisms in microalgal control of cell propagation, metabolic acclimation (including accumulation of TAG), and maintenance of chlorophyll

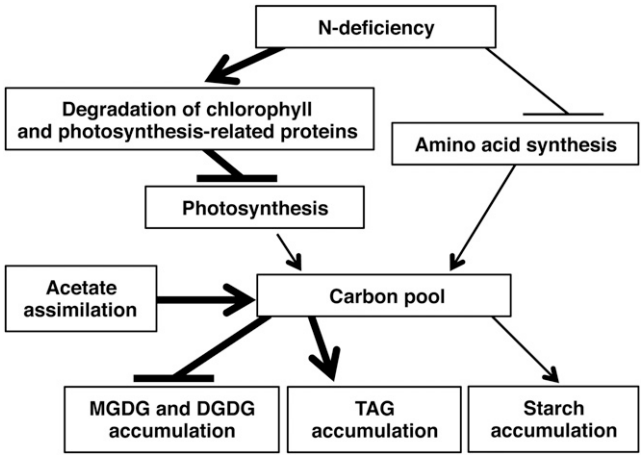

Figure 9. A hypothetical model of functional roles of TAR1 on the cellular responses to N deficiency in the photomixotrophic culture conditions. Possible positively and negatively controlled steps by TAR1 in wild-type cells in N-deficient conditions are indicated by bold arrows and bold lines, respectively.

molecules. Characterization of *tar1* mutants in land plants would also help us to understand the biological functions of DYRKs in response to different stresses, such as nutrient deficiency in photosynthetic eukaryotes.

MATERIALS AND METHODS

Strains and Culture Conditions

Green alga (*Chlamydomonas reinhardtii*) strain C-9 (mt^-), which is a wild-type strain in terms of lipid metabolism (Kajikawa et al., 2006; Iwai et al., 2014), was originally from the Institute of Applied Microbiology Culture Collection and is presently available from the National Institute for Environmental Studies as NIES-2235. Strain CC-125 (mt^-) from the Chlamydomonas Resource Center (University of Minnesota) was used for genetic analysis. Tetrad progenies were isolated from the cross between *tar1-1* (mt^-) and wild-type strain CC-125 (mt^+) as described previously (Harris, 2009; Wang et al., 2014). For studies of S deficiency, cells in late logarithmic phase (approximately 8.0×10^6 cells mL^{-1}) were centrifuged at 600*g* for 5 min at room temperature. Then, cell pellets were washed two times in TAP − S medium (Harris, 2009), resuspended in 100 mL of TAP − S medium, and further cultured at 60 μmol photons m^{-2} s^{-1} for 2 d. For studies of N deficiency, similar to the S-deficient culture, cells in late logarithmic phase were collected and washed two times in TAP − N medium (Harris, 2009). The cells were resuspended and further cultured in 100 mL of TAP − N medium for 2 d. The cell number was counted using Automatic Cell Counter TC20 (Bio-Rad). The cell volume was measured using the particle analyzer CDA-1000 (Sysmex). Cell densities were estimated by measuring A_{730}.

Measurement of Chlorophyll Content and Cell Viability

Chlorophyll was extracted from a fresh cell pellet using 95% (v/v) ethanol, and chlorophyll concentrations were calculated from absorbance values at 649 and 665 nm (Wintermans and de Mots, 1965). Cell viability was measured by the Evans Blue staining method as described by Pérez-Martín et al. (2014).

Transformation of *C. reinhardtii* Cells

To prepare *C. reinhardtii* transformant pools for FACS-mediated mutant screening, a 1,999-bp PCR fragment containing the hygromycin resistance gene *aph7* expressed from the β2-tublin promoter was used to transform C-9 cells without cell wall removal as described previously (Yamano et al., 2013; Wang et al., 2014). TAP solid medium containing 30 mg L^{-1} of hygromycin (Wako) was used for selection.

For complementation analysis of *tar1-1*, a 15-kb genomic DNA fragment containing the *TAR1* coding region with 1 kb of its own promoter was amplified by PCR with primers Pro-F and Stop-R using fosmid clone GCRFno11_b05 containing the *TAR1* genomic DNA as a template. The PCR product was cloned into the *Spe*I/*Bgl*II sites of a pGenD-HA expression vector carrying a paromomycin resistance gene (Nakazawa et al., 2007) using the In-Fusion Reaction (Takara Bio). The resultant plasmid, pGenD-TAR1, was linearized using *Spe*I (New England Biolabs) and used to transform *tar1-1*. Paromomycin-resistant clones were selected on TAP solid medium containing 10 mg L^{-1} of paromomycin (Wako). Clones carrying the wild-type *TAR1* gene sequence were screened for *tar1-1* by genomic PCR with primers TAR1-01F and TAR1-01R. PCR-positive clones were cultured in N-deficient conditions, and we examined the *TAR1* transcript level and amount of TAG accumulation. Nucleotide sequences of the primers are listed in Supplemental Table S2.

FACS Analysis

Approximately 1 to 2×10^7 cells transformed with the hygromycin resistance cassette grown for 2 d in S-deficient conditions were stained with 1 μM 4,4-difluoro-3a,4a-diaza-s-indacene (BODIPY 493/503; Life Technologies) by incubating for over 10 min at room temperature and flow sorting using BD FACSAria (Becton Dickinson). A 488-nm semiconductor laser was used for excitation, and 530-/30-nm (fluorescein isothiocyanate-A channel) and 695-/40-nm (PerCP-Cy5-5A channel) emission filters were used to image BODIPY 493/503 and chlorophyll fluorescence, respectively. Scatter plots of BODIPY 493/503 versus chlorophyll fluorescence were used to establish a gate for isolating candidate low TAG-accumulating mutants (Fig. 1A). Approximately 10,000 sorted cells were collected and suspended in 100 mL of TAP medium containing 500 μg mL^{-1} of ampicillin and cultured for 1 week. Then, the cells were incubated in TAP − S medium for 2 d and resorted to concentrate mutants with the low levels of TAG accumulation.

Molecular Techniques

To identify the insertion locus of the DNA tag in *tar1-1*, thermal asymmetric interlaced PCR was performed as described previously (Wang et al., 2014). To determine the sequence of the *TAR1* cDNA by quantitative real-time PCR and RNA-seq analysis, total RNA was extracted from wild-type, *tar1-1*, and C1 cells 6 h after being transferred to TAP − N, TAP − S, and normal TAP medium using an RNeasy Plant Mini Kit (QIAGEN), and any remaining genomic DNA was digested using RNase-free DNase (QIAGEN) in accordance with the manufacturer's instructions. The 5′ and 3′ regions of the *TAR1* cDNA were obtained using a SMARTer RACE cDNA Amplification Kit (Takara Bio). Quantitative real-time PCR was performed using SYBR Premix Ex Taq GC (Takara Bio) and a LightCycler 480 Instrument (Roche) as described previously (Wang et al., 2014). The cryptopleurine resistance gene (*CRY1*)-encoding ribosomal protein S14 was used as an internal control (Lin et al., 2010). The primers used for quantitative reverse transcription (qRT)-PCR are described in Supplemental Table S6.

Immunoblotting Analysis

Immunoblotting analysis was performed as described previously (Wang et al., 2014). The following antibodies were used: anti-rbcL (1:5,000 dilution), anticytochrome *f* (1:5,000 dilution; provided by Yuichiro Takahashi, Okayama University, Okayama, Japan), and anti-α-tubulin (1:5,000 dilution; T5168; Sigma-Aldrich). A horseradish peroxidase-linked goat anti-rabbit IgG antibody (1:10,000 dilution; GE Healthcare Life Sciences) for rbcL and cytochrome *f* detection and horseradish peroxidase-conjugated goat anti-mouse IgG antibody (1:10,000 dilution; GE Healthcare Life Sciences) for α-tubulin detection were used as secondary antibodies. Tris-buffered saline with 0.05% (v/v) Triton X-100 was used for dilution of these antibodies.

RNA-Seq Analysis

RNA was quantified using a 2100 Bio-Analyzer (Agilent Technologies). At least 20 μg of total RNA at a concentration of 250 ng μL^{-1} was used for cDNA library preparation using an Illumina TruSeq RNA Sample Prep Kit. The library was validated on a 2100 Bio-Analyzer (Agilent Technologies) and an ABI StepOnePlus Real-Time PCR System (Life Technologies). Illumina HiSeq 2000 sequencing was performed at the Beijing Genome Institute. Sequencing reads were mapped to green alga transcripts (version 5.5) deposited in the Phytozome database using the bowtie software package (Langmead et al., 2009). No more than two mismatches per sequencing were allowed. In each condition, the reads per kilobase of transcript per million reads mapped (RPKMs) of two biological replicates were averaged. For those genes with null RPKM values, a value equal to the minimum in each experiment was applied. DEGs between N-deficient and -replete conditions in each line and DEGs among the wild type, *tar1-1*, and C1 in N-deficient conditions were evaluated by calculating the *q* values using the Bioconducter package DESeq (Anders and Huber, 2010).

Measurement of Photosynthetic Activity

Cells were collected by centrifugation and then resuspended in inorganic carbon-deficient 50 mM HEPES-NaOH buffer (pH 7.8) at 15 μg mL^{-1} chlorophyll. The maximum rate of inorganic carbon-dependent, O_2-evolving activity, defined as V_{max}, was measured using a Clark-type O_2 electrode (Hansatech Instruments) as described previously (Yamano et al., 2008) in the presence of 10 mM $NaHCO_3$.

Lipid Analysis

Total lipids were extracted in a chloroform-methanol-water system (Bligh and Dyer, 1959). Neutral lipids were separated into sterol esters, monoacylglycerol, diacylglycerol, and TAG by thin-layer chromatography (TLC) using silica plates (TLC silica gel 60; 20 × 20 cm; Merck Millipore) developed with *n*-hexane:diethyl ether:acetic acid (70:30:1, v/v). After drying, the plate was

sprayed with 80% (v/v) aqueous acetone containing 0.01% (w/v) primuline. The amount of TAG was quantified by gas chromatography-mass spectrometry after derivatization to fatty acid methyl esters using heptadecanoic acid (C17:0) as the internal standard (Chen et al., 2008). Lipid classes were separated by two-dimensional TLC, and their contents were quantified by gas chromatography-mass spectrometry as described previously (Li et al., 2010; Sakurai et al., 2014).

To estimate the relative amount of neutral lipids, a 200-μL sample of each N-deficient cell culture was mixed with 5 μL of AdipoRed solution (Lonza) and incubated for 5 min in the dark to stain neutral lipids. Fluorescence at 485 nm excitation with a 555-nm emission filter was read using a Fluoroskan Ascent Microplate Fluorometer (Thermo Fisher Scientific). The neutral lipid-specific signal was calculated as (AdipoRed fluorescence − background fluorescence)/cell density at 730 nm.

Quantitative Analysis of Starch and Acetate

For quantitative analysis of intracellular starch, cells in 5 mL of culture were harvested by centrifugation (13,000*g* for 5 min at 4°C) and then suspended in ethanol. After boiling for 30 min at 95°C, the suspension was centrifuged (13,000*g* for 5 min at 4°C), and the cell pellet was dried. Then, the pellet was boiled with 1 mL of 0.2 M KOH for 30 min. To this extract, 0.2 mL of 1 M acetic acid was added to adjust the pH to 5.5. The extract was treated with α-amylase and amyloglucosidase using a Total Starch Assay Kit (AA/AMG; Megazyme). After D-Glc oxidization by Glc oxidase, 1 mol of hydrogen peroxide is released. Levels of hydrogen peroxide were determined using a colorimetric reaction using peroxidase and the production of a quinoneimine dye (Izumo et al., 2007).

For quantitative analysis of acetate in the culture medium, 1 mL of cell culture was centrifuged at 4°C for 1 min, and acetate concentration in the supernatants was measured using enzymatic assays (F-Kit; Roche).

Confocal and Electron Microscopy

Images of stained cells were captured using a Leica TCS SP8 Microscope (Leica Microsystems). For neutral lipid-specific detection of AdipoRed fluorescence, a 488-nm argon laser was used for excitation, and fluorescence between 500 and 550 nm and between 705 and 765 nm was detected as fluorescence from AdipoRed and chlorophyll, respectively. For the measurement of the apparent diameter of LDs, micrographs were analyzed using LAS AF software (Leica Microsystems).

For electron microscopic analysis, cells were fixed with 2% (v/v) glutaraldehyde in 0.1 M phosphate buffer (pH 7.4) at 4°C and postfixed with 2% (w/v) osmium tetroxide. After fixation, the cells were dehydrated in an ethanol series, exchanged for propylene oxide, and embedded in epoxy resin (Quetol 812; Nisshin EM). Ultrathin sections (80 to 90 nm thick) were cut using an ultramicrotome (ULTRACUTS; Leica Microsystems) and then stained with 2% (v/v) aqueous uranyl acetate and lead staining solution. Transmission electron micrographs were captured using a JEM-1200EX at 80 kV (JEOL).

Expression of Recombinant TAR1 Proteins and Kinase Assays

For kinase assays, recombinant partial proteins (TAR1 and TAR1^{KD}) were expressed as fusions with a His-Trigger Factor tag from a pCold TF vector (Takara Bio) in *Escherichia coli* strain BL21(DE3) pLysS (BioDynamics Laboratory) and purified using a HisTALON Gravity Column (Takara Bio). For removal of the His-Trigger Factor tag at the N terminus, the proteins were digested with HRV 3C protease and purified by binding with cOmplete His-Tag Purification Resin (Roche).

Kinase assays were carried out as follows. Reaction mixtures containing 80 mM K-phosphate (pH 7.5), 20 mM $MgCl_2$, 100 μM ATP, 370 kBq of [γ-^{32}P]ATP (222 TBq mmol^{-1}; Perkin Elmer), 0.5 μg of purified recombinant proteins (TAR1 or TAR1^{KD}), and substrate protein 0.2 μg of casein (C7078; Sigma), 0.2 μg of MBP (M1819; Sigma), or 5 μg of histone type III-S (H5505; Sigma) were incubated for 30 min at 30°C and then separated by SDS-PAGE. After staining with Coomassie Brilliant Blue, the phosphorylated proteins were detected using an imaging analyzer Typhoon FLA7000 (GE Healthcare Life Sciences). Autophosphorylation assays were performed in the same manner but without substrate.

The nucleotide sequence of the *TAR1* gene from this article can be found in the DNA Data Bank of Japan (DDBJ)/GenBank/European Molecular Biology Laboratory database under accession number AB971117, and RNA-seq raw data (Supplemental Data Sets S1–S7) from this article can be found in the DDBJ Sequenced Read Archive under accession number DRA002413.

Supplemental Data

The following supplemental materials are available.

Supplemental Figure S1. Average number and size distribution of LDs in the wild-type, *tar1-1*, and C1 cells cultured for 2 d in N-deficient conditions.

Supplemental Figure S2. Structure of TAR1.

Supplemental Figure S3. Genetic analysis of *tar1-1*.

Supplemental Figure S4. Levels of lipids and starch in S deficiency.

Supplemental Figure S5. Phenotypic changes of the wild type, *tar1-1*, and C1 after transfer to S-deficient conditions.

Supplemental Figure S6. Cell viability of the wild-type and *tar1-1* cells in S-deficient and N-deficient conditions estimated by Evans Blue staining.

Supplemental Figure S7. Doubling times of the wild-type, *tar1-1*, and C1 cells in nutrient-replete conditions.

Supplemental Table S1. Summary of RNA-seq samples and sequence alignment.

Supplemental Table S2. Already annotated genes in group a in Figure 7 with RPKMs in the wild type in N-deficient conditions that were significantly larger than those in *tar1-1* in N-deficient conditions.

Supplemental Table S3. Already annotated genes in group b in Figure 7 with RPKMs in *tar1-1* in N-deficient conditions that were significantly larger than those in the wild type during N deficiency.

Supplemental Table S4. Already annotated genes in group f in Figure 7 with RPKMs in the wild type in N-deficient conditions that were significantly smaller than those in *tar1-1* during N deficiency.

Supplemental Table S5. Accession numbers of DYRK sequences used for the phylogenetic tree in Figure 8.

Supplemental Table S6. Primer sequences.

Supplemental Data Set S1. Overview of RNA-seq experiments (all genes).

Supplemental Data Set S2. DEGs up-regulated in N-deficient conditions in both the wild type and C1 but not *tar1-1*.

Supplemental Data Set S3. DEGs up-regulated in N-deficient conditions in *tar1-1* but not the wild type and C1.

Supplemental Data Set S4. DEGs up-regulated in N-deficient conditions in all of the wild type, C1, and *tar1-1*.

Supplemental Data Set S5. DEGs down-regulated in N-deficient conditions in both the wild type and C1 but not *tar1-1*.

Supplemental Data Set S6. DEGs down-regulated in N-deficient conditions in *tar1-1* but not the wild type and C1.

Supplemental Data Set S7. DEGs down-regulated in N-deficient conditions in all of the wild type, C1, and *tar1-1*.

ACKNOWLEDGMENTS

We thank Yoshihiko Fujita, Tan Inoue (Kyoto University), Yoko Ide, and Sigeaki Harayama (Chuo University, Japan) for technical support on the FACS analysis and Yuichiro Takahashi (Okayama University, Japan) for providing the anticytochrome *f* antibody.

Received March 1, 2015; accepted April 24, 2015; published April 28, 2015.

LITERATURE CITED

Anders S, Huber W (2010) Differential expression analysis for sequence count data. Genome Biol **11:** R106

Aranda S, Laguna A, de la Luna S (2011) DYRK family of protein kinases: evolutionary relationships, biochemical properties, and functional roles. FASEB J **25:** 449–462

Becker W (2012) Emerging role of DYRK family protein kinases as regulators of protein stability in cell cycle control. Cell Cycle **11:** 3389–3394

Bellou S, Aggelis G (2012) Biochemical activities in *Chlorella* sp. and *Nannochloropsis salina* during lipid and sugar synthesis in a lab-scale open pond simulating reactor. J Biotechnol **164:** 318–329

Blaby IK, Glaesener AG, Mettler T, Fitz-Gibbon ST, Gallaher SD, Liu B, Boyle NR, Kropat J, Stitt M, Johnson S, et al (2013) Systems-level analysis of nitrogen starvation-induced modifications of carbon metabolism in a *Chlamydomonas reinhardtii* starchless mutant. Plant Cell **25:** 4305–4323

Bligh EG, Dyer WJ (1959) A rapid method of total lipid extraction and purification. Can J Biochem Physiol **37:** 911–917

Boyle NR, Page MD, Liu B, Blaby IK, Casero D, Kropat J, Cokus SJ, Hong-Hermesdorf A, Shaw J, Karpowicz SJ, et al (2012) Three acyltransferases and nitrogen-responsive regulator are implicated in nitrogen starvation-induced triacylglycerol accumulation in *Chlamydomonas*. J Biol Chem **287:** 15811–15825

Chen GQ, Jiang Y, Chen F (2008) Salt-induced alterations in lipid composition of diatom *Nitzschia laevis* (Bacillariophyceae) under heterotrophic culture condition. J Phycol **44:** 1309–1314

Daboussi F, Leduc S, Maréchal A, Dubois G, Guyot V, Perez-Michaut C, Amato A, Falciatore A, Juillerat A, Beurdeley M, et al (2014) Genome engineering empowers the diatom *Phaeodactylum tricornutum* for biotechnology. Nat Commun **5:** 3831

Fan J, Yan C, Andre C, Shanklin J, Schwender J, Xu C (2012) Oil accumulation is controlled by carbon precursor supply for fatty acid synthesis in *Chlamydomonas reinhardtii*. Plant Cell Physiol **53:** 1380–1390

Fernández E, Llamas Á, Galván A (2009) Nitrogen assimilation and its regulation. *In* D Stern, EH Harris, eds, The Chlamydomonas Source Book. Vol. 2: Organellar and Metabolic Processes, Ed 2. Elsevier, Dordrecht, The Netherlands, pp 69–113

Goodson C, Roth R, Wang ZT, Goodenough U (2011) Structural correlates of cytoplasmic and chloroplast lipid body synthesis in Chlamydomonas reinhardtii and stimulation of lipid body production with acetate boost. Eukaryot Cell **10:** 1592–1606

Guimerá J, Casas C, Pucharcòs C, Solans A, Domènech A, Planas AM, Ashley J, Lovett M, Estivill X, Pritchard MA (1996) A human homologue of *Drosophila minibrain* (*MNB*) is expressed in the neuronal regions affected in Down syndrome and maps to the critical region. Hum Mol Genet **5:** 1305–1310

Harris EH (2009) *Chlamydomonas* in the laboratory. *In* D Stern, EH Harris, eds, The Chlamydomonas Source Book. Vol. 1: Introduction to *Chlamydomonas* and Its Laboratory Use, Ed 2. Elsevier, Dordrecht, The Netherlands, pp 241–302

Ho CH, Lin SH, Hu HC, Tsay YF (2009) CHL1 functions as a nitrate sensor in plants. Cell **138:** 1184–1194

Hu HC, Wang YY, Tsay YF (2009) AtCIPK8, a CBL-interacting protein kinase, regulates the low-affinity phase of the primary nitrate response. Plant J **57:** 264–278

Iwai M, Ikeda K, Shimojima M, Ohta H (2014) Enhancement of extraplastidic oil synthesis in *Chlamydomonas reinhardtii* using a type-2 diacylglycerol acyltransferase with a phosphorus starvation-inducible promoter. Plant Biotechnol J **12:** 808–819

Izumo A, Fujiwara S, Oyama Y, Satoh A, Fujita N, Nakamura Y, Tsuzuki M (2007) Physicochemical properties of starch in *Chlorella* change depending on the CO_2 concentration during growth: comparison of structure and properties of pyrenoid and stroma starch. Plant Sci **172:** 1138–1147

Jobb G, von Haeseler A, Strimmer K (2004) TREEFINDER: a powerful graphical analysis environment for molecular phylogenetics. BMC Evol Biol **4:** 18

Johnson X, Alric J (2013) Central carbon metabolism and electron transport in *Chlamydomonas reinhardtii*: metabolic constraints for carbon partitioning between oil and starch. Eukaryot Cell **12:** 776–793

Kajikawa M, Yamato KT, Kohzu Y, Shoji S, Matsui K, Tanaka Y, Sakai Y, Fukuzawa H (2006) A front-end desaturase from *Chlamydomonas reinhardtii* produces pinolenic and coniferonic acids by ω13 desaturation in methylotrophic yeast and tobacco. Plant Cell Physiol **47:** 64–73

Kroll D, Meierhoff K, Bechtold N, Kinoshita M, Westphal S, Vothknecht UC, Soll J, Westhoff P (2001) *VIPP1*, a nuclear gene of *Arabidopsis thaliana* essential for thylakoid membrane formation. Proc Natl Acad Sci USA **98:** 4238–4242

Langmead B, Trapnell C, Pop M, Salzberg SL (2009) Ultrafast and memory-efficient alignment of short DNA sequences to the human genome. Genome Biol **10:** R25

Lee P, Cho BR, Joo HS, Hahn JS (2008) Yeast Yak1 kinase, a bridge between PKA and stress-responsive transcription factors, Hsf1 and Msn2/Msn4. Mol Microbiol **70:** 882–895

Li X, Moellering ER, Liu B, Johnny C, Fedewa M, Sears BB, Kuo MH, Benning C (2012) A galactoglycerolipid lipase is required for triacylglycerol accumulation and survival following nitrogen deprivation in *Chlamydomonas reinhardtii*. Plant Cell **24:** 4670–4686

Li Y, Han D, Hu G, Dauvillee D, Sommerfeld M, Ball S, Hu Q (2010) *Chlamydomonas* starchless mutant defective in ADP-glucose pyrophosphorylase hyper-accumulates triacylglycerol. Metab Eng **12:** 387–391

Lin H, Kwan AL, Dutcher SK (2010) Synthesizing and salvaging NAD: lessons learned from *Chlamydomonas reinhardtii*. PLoS Genet **6:** e1001105

Longworth J, Noirel J, Pandhal J, Wright PC, Vaidyanathan S (2012) HILIC- and SCX-based quantitative proteomics of *Chlamydomonas reinhardtii* during nitrogen starvation induced lipid and carbohydrate accumulation. J Proteome Res **11:** 5959–5971

Martin DE, Soulard A, Hall MN (2004) TOR regulates ribosomal protein gene expression via PKA and the Forkhead transcription factor FHL1. Cell **119:** 969–979

Merchant SS, Kropat J, Liu B, Shaw J, Warakanont J (2012) TAG, you're it! Chlamydomonas as a reference organism for understanding algal triacylglycerol accumulation. Curr Opin Biotechnol **23:** 352–363

Merchant SS, Prochnik SE, Vallon O, Harris EH, Karpowicz SJ, Witman GB, Terry A, Salamov A, Fritz-Laylin LK, Maréchal-Drouard L, et al (2007) The *Chlamydomonas* genome reveals the evolution of key animal and plant functions. Science **318:** 245–250

Miller R, Wu G, Deshpande RR, Vieler A, Gärtner K, Li X, Moellering ER, Zäuner S, Cornish AJ, Liu B, et al (2010) Changes in transcript abundance in *Chlamydomonas reinhardtii* following nitrogen deprivation predict diversion of metabolism. Plant Physiol **154:** 1737–1752

Moriya H, Shimizu-Yoshida Y, Omori A, Iwashita S, Katoh M, Sakai A (2001) Yak1p, a DYRK family kinase, translocates to the nucleus and phosphorylates yeast Pop2p in response to a glucose signal. Genes Dev **15:** 1217–1228

Nakazawa Y, Hiraki M, Kamiya R, Hirono M (2007) SAS-6 is a cartwheel protein that establishes the 9-fold symmetry of the centriole. Curr Biol **17:** 2169–2174

Nordhues A, Schöttler MA, Unger AK, Geimer S, Schönfelder S, Schmollinger S, Rütgers M, Finazzi G, Soppa B, Sommer F, et al (2012) Evidence for a role of VIPP1 in the structural organization of the photosynthetic apparatus in *Chlamydomonas*. Plant Cell **24:** 637–659

Park JJ, Wang H, Gargouri M, Deshpande RR, Skepper JN, Holguin FO, Juergens MT, Shachar-Hill Y, Hicks LM, Gang DR (2015) The response of *Chlamydomonas reinhardtii* to nitrogen deprivation: a systems biology analysis. Plant J **81:** 611–624

Pérez-Martín M, Pérez-Pérez ME, Lemaire SD, Crespo JL (2014) Oxidative stress contributes to autophagy induction in response to endoplasmic reticulum stress in *Chlamydomonas reinhardtii*. Plant Physiol **166:** 997–1008

Riekhof WR, Benning C (2009) Glycerolipids biosynthesis. *In* D Stern, EH Harris, eds, The Chlamydomonas Source Book. Vol. 2: Organellar and Metabolic Processes, Ed 2. Elsevier, Dordrecht, The Netherlands, pp 41–68

Sakurai K, Moriyama T, Sato N (2014) Detailed identification of fatty acid isomers sheds light on the probable precursors of triacylglycerol accumulation in photoautotrophically grown *Chlamydomonas reinhardtii*. Eukaryot Cell **13:** 256–266

Sato A, Matsumura R, Hoshino N, Tsuzuki M, Sato N (2014) Responsibility of regulatory gene expression and repressed protein synthesis for triacylglycerol accumulation on sulfur-starvation in *Chlamydomonas reinhardtii*. Front Plant Sci **5:** 444

Schmollinger S, Mühlhaus T, Boyle NR, Blaby IK, Casero D, Mettler T, Moseley JL, Kropat J, Sommer F, Strenkert D, et al (2014) Nitrogen-sparing mechanisms in *Chlamydomonas* affect the transcriptome, the proteome, and photosynthetic metabolism. Plant Cell **26:** 1410–1435

Siaut M, Cuiné S, Cagnon C, Fessler B, Nguyen M, Carrier P, Beyly A, Beisson F, Triantaphylidès C, Li-Beisson Y, et al (2011) Oil accumulation in the model green alga *Chlamydomonas reinhardtii*: characterization, variability between common laboratory strains and relationship with starch reserves. BMC Biotechnol **11:** 7

Spalding MH (2009) The CO_2-concentrating mechanism and carbon assimilation. *In* D Stern, EH Harris, eds, The Chlamydomonas Source Book. Vol. 2: Organellar and Metabolic Processes, Ed 2. Elsevier, Dordrecht, The Netherlands, pp 257–301

Vallon O, Spalding MH (2009) Amino acid metabolism. *In* D Stern, EH Harris, eds, The Chlamydomonas Source Book. Vol. 2: Organellar and Metabolic Processes, Ed 2. Elsevier, Dordrecht, The Netherlands, pp 115–158

Wang J, Zhang H, Allen RD (1999) Overexpression of an *Arabidopsis* peroxisomal ascorbate peroxidase gene in tobacco increases protection against oxidative stress. Plant Cell Physiol **40:** 725–732

Wang L, Yamano T, Kajikawa M, Hirono M, Fukuzawa H (2014) Isolation and characterization of novel high-CO_2-requiring mutants of *Chlamydomonas reinhardtii*. Photosynth Res **121:** 175–184

Wei L, Derrien B, Gautier A, Houille-Vernes L, Boulouis A, Saint-Marcoux D, Malnoë A, Rappaport F, de Vitry C, Vallon O, et al (2014) Nitric oxide-triggered remodeling of chloroplast bioenergetics and thylakoid proteins upon nitrogen starvation in *Chlamydomonas reinhardtii*. Plant Cell **26:** 353–372

Wintermans JF, de Mots A (1965) Spectrophotometric characteristics of chlorophylls *a* and *b* and their pheophytins in ethanol. Biochim Biophys Acta **109:** 448–453

Work VH, Radakovits R, Jinkerson RE, Meuser JE, Elliott LG, Vinyard DJ, Laurens LM, Dismukes GC, Posewitz MC (2010) Increased lipid accumulation in the *Chlamydomonas reinhardtii sta7-10* starchless isoamylase mutant and increased carbohydrate synthesis in complemented strains. Eukaryot Cell **9:** 1251–1261

Yamano T, Iguchi H, Fukuzawa H (2013) Rapid transformation of *Chlamydomonas reinhardtii* without cell-wall removal. J Biosci Bioeng **115:** 691–694

Yamano T, Miura K, Fukuzawa H (2008) Expression analysis of genes associated with the induction of the carbon-concentrating mechanism in *Chlamydomonas reinhardtii*. Plant Physiol **147:** 340–354

Yoon K, Han D, Li Y, Sommerfeld M, Hu Q (2012) Phospholipid:diacylglycerol acyltransferase is a multifunctional enzyme involved in membrane lipid turnover and degradation while synthesizing triacylglycerol in the unicellular green microalga *Chlamydomonas reinhardtii*. Plant Cell **24:** 3708–3724

Yoshida K (2008) Role for DYRK family kinases on regulation of apoptosis. Biochem Pharmacol **76:** 1389–1394

Zhang JQ, He GJ, Yan YB (2013) Biochemical and biophysical characterization of the deadenylase CrCaf1 from *Chlamydomonas reinhardtii*. PLoS ONE **8:** e69582